

# Preparation and characterization of a silica-based magnetic nanocomposite and its application as a recoverable catalyst for the one-pot multicomponent synthesis of quinazolinone derivatives

Ali Maleki\*, Mahboubeh Rabbani and Shirin Shahrokh



An environmentally benign magnetic silica-based nanocomposite ( $\text{Fe}_3\text{O}_4/\text{SBA-15}$ ) as a heterogeneous nanocatalyst was prepared and characterized using Fourier transform infrared and ultraviolet–visible diffuse reflectance spectroscopies, scanning electron microscopy, X-ray diffraction, vibrating sample magnetometry and Brunauer–Emmett–Teller multilayer nitrogen adsorption. Its catalytic activity was investigated for the one-pot multicomponent synthesis of 2,3-dihydroquinazolin-4(1*H*)-ones starting from isatoic anhydride, ammonium acetate and various aldehydes under mild reaction conditions and easy work-up procedure in refluxing ethanol with good yields. The nanocatalyst can be recovered easily and reused several times without significant loss of catalytic activity. Copyright © 2015 John Wiley & Sons, Ltd.

Additional supporting information may be found in the online version of this article at the publisher's web-site.

**Keywords:** composite nanostructures; magnetic nanocatalyst;  $\text{Fe}_3\text{O}_4$  nanoparticles; SBA-15; multicomponent reaction

## Introduction

Magnetic iron oxide nanoparticles are particularly attractive owing to their unique properties and potential applications in various fields.<sup>[1]</sup> In general, the naked nanoparticles tend to aggregate into large clusters. This problem can be overcome by immobilizing the nanoparticles on substrates such as polymers, carbons and mesoporous silica.<sup>[2]</sup> SBA-15, as a highly ordered mesoporous material, is one of the best substrates for this purpose, due to its large surface area, high chemical and thermal stability and good compatibility.<sup>[3]</sup> The integration of mesoporous silica with magnetic nanoparticles to form porous magnetic nanocomposites is undoubtedly of great interest for practical applications. These types of magnetic nanocomposites have the advantages of both mesoporous silica and magnetic nanoparticles. In recent years, several studies have been done on the synthesis and application of these magnetic nanocomposites in organic manufacturing.<sup>[4]</sup>

Quinazoline derivatives are an important class of heterocyclic compounds that have diverse biological and pharmaceutical properties such as antifertility, antibacterial, antiviral, antitumor and antifungal activities.<sup>[5]</sup> Quinazolin-4(3*H*)-one analogues as important pharmacologically active compounds<sup>[6]</sup> have been synthesized using several methods.<sup>[7–24]</sup> The most common procedure involves the condensation reaction of anthranilamide with aldehydes or ketones using various catalysts such as  $\text{TiCl}_4\text{-Zn}$ ,<sup>[7]</sup>  $\text{Sc}(\text{OTf})_3$ ,<sup>[8]</sup>  $\text{NH}_4\text{Cl}$ ,<sup>[9]</sup>  $\text{HCl}$ ,<sup>[10]</sup> *p*-toluenesulfonic acid (PTSA),<sup>[11]</sup>  $\text{SmI}_2$ ,<sup>[12]</sup>  $\text{CuCl}_2$ ,<sup>[13]</sup>  $\text{MnO}_2$ ,<sup>[14]</sup>  $\text{KMnO}_4$ ,<sup>[15]</sup> ionic liquid or 2,2,2-trifluoroethanol without additional catalyst<sup>[16]</sup> and copper-catalysed Ullmann *N*-arylation coupling process.<sup>[17]</sup>

Several strategies for the synthesis of 2,3-dihydroquinazolinone derivatives involve a one-pot three-component condensation of

isatoic anhydride, aldehydes and amines or ammonium acetate using catalysts such as  $\text{Ga}(\text{OTf})_3$ ,<sup>[18]</sup>  $\text{Bi}(\text{NO}_3)_3\cdot 5\text{H}_2\text{O}$ ,<sup>[19]</sup>  $\text{KAl}(\text{SO}_4)_2\cdot 12\text{H}_2\text{O}$ ,<sup>[20]</sup> PTSA,<sup>[21]</sup>  $\text{Fe}_3\text{O}_4$ ,<sup>[22]</sup>  $\text{SrCl}_2\cdot 6\text{H}_2\text{O}$ <sup>[23]</sup> and  $\text{Cu}(\text{C}_6\text{H}_5\text{SO}_3)_2\cdot 6\text{H}_2\text{O}$ .<sup>[24]</sup>

In continuation of our recent researches towards the development of green, simple and environmentally benign protocols in organic reactions,<sup>[25]</sup> herein, for the first time, we introduce a magnetite–silica nanocomposite ( $\text{Fe}_3\text{O}_4/\text{SBA-15}$ ) as an efficient nanocatalyst in multicomponent reactions (MCRs) for the one-pot synthesis of 2,3-dihydroquinazolin-4(1*H*)-one derivatives **4a–g** using isatoic anhydride (**1**), ammonium acetate (**2**) and various aldehydes (**3**) in refluxing ethanol in good to excellent yields (Scheme 1). To the best of our knowledge, this is the first synthesis of dihydroquinazolinones catalysed by superparamagnetic composite nanoparticles via MCRs.

## Results and discussion

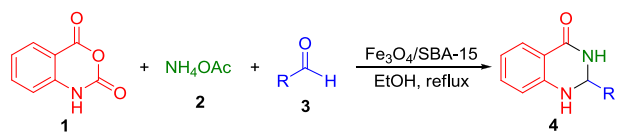
### Characterization of nanocatalyst

Fourier transform infrared (FT-IR) spectroscopy of  $\text{Fe}_3\text{O}_4/\text{SBA-15}$

The FT-IR spectra of neat SBA-15, neat  $\text{Fe}_3\text{O}_4$  and  $\text{Fe}_3\text{O}_4/\text{SBA-15}$  samples are shown in Fig. 1. Their comparison confirms the efficient

\* Correspondence to: Ali Maleki, Catalysts and Organic Synthesis Research Laboratory, Department of Chemistry, Iran University of Science and Technology, Tehran 16846-13114, Iran. E-mail: maleki@iust.ac.ir

Catalysts and Organic Synthesis Research Laboratory, Department of Chemistry, Iran University of Science and Technology, Tehran 16846-13114, Iran



**Scheme 1.**  $\text{Fe}_3\text{O}_4/\text{SBA-15}$ -catalysed synthesis of 2,3-dihydroquinazolin-4(1*H*)-ones **4a–j**.

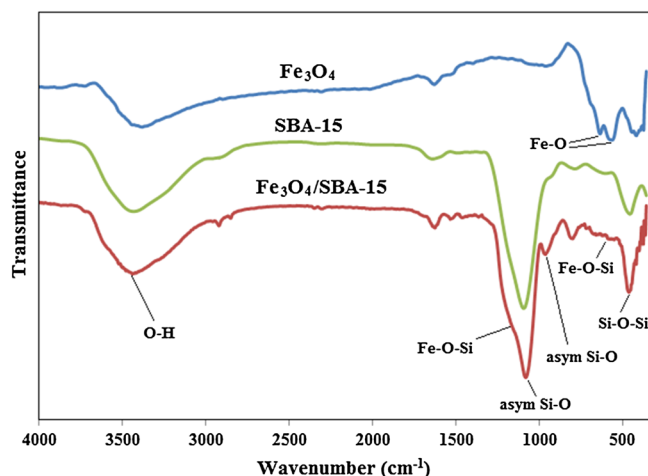


**Figure 1.** FT-IR spectra of neat SBA-15, neat  $\text{Fe}_3\text{O}_4$  and  $\text{Fe}_3\text{O}_4/\text{SBA-15}$ .

loading of  $\text{Fe}_3\text{O}_4$  nanoparticles on SBA-15 and the formation of the magnetic composite nanocatalyst. For neat  $\text{Fe}_3\text{O}_4$ , the bands at 561 and 640  $\text{cm}^{-1}$  are ascribed to Fe–O of iron oxide nanoparticles. In the FT-IR spectrum of neat SBA-15, the symmetric and asymmetric stretching vibration bands of Si–O–Si bond are observed at 810 and 1093  $\text{cm}^{-1}$ , respectively. The peak at 452  $\text{cm}^{-1}$  is assigned to the Si–O–Si bending vibration. A broad band around 3440  $\text{cm}^{-1}$  is assigned to stretching vibration of O–H in water molecules adsorbed on the surface and the stretching vibration of surface silanol groups. After the loading of  $\text{Fe}_3\text{O}_4$  nanoparticles on SBA-15, bands at 640 and 1150  $\text{cm}^{-1}$  can be attributed to the Fe–O–Si bond.<sup>4c)</sup> However, the presence of Fe–O–Si bonds cannot be seen clearly in the FT-IR spectrum because the band overlaps with the Si–O vibration of neat SBA-15.

#### X-ray diffraction (XRD) analysis of $\text{Fe}_3\text{O}_4/\text{SBA-15}$

The structure of the as-synthesized  $\text{Fe}_3\text{O}_4$  inside SBA-15 was investigated using XRD. Figure 2(A) shows wide-angle XRD patterns of neat SBA-15,  $\text{Fe}_3\text{O}_4$  and  $\text{Fe}_3\text{O}_4/\text{SBA-15}$  samples. The diffraction peaks observed at 30.00°, 35.48°, 43.14°, 53.44°, 57.04° and 62.58° are well indexed to the cubic spinel structure of pure  $\text{Fe}_3\text{O}_4$  (JCPDS file no. 19-0629). No peaks of iron hydroxide, hematite or other impurities are detected, suggesting the complete formation of magnetite, and also the strong and sharp peaks reveal that the  $\text{Fe}_3\text{O}_4$  particles are well crystallized. For the neat SBA-15 and  $\text{Fe}_3\text{O}_4/\text{SBA-15}$ , the broad diffraction peak between 20° and 30° is attributed to the silicon material. In addition, the results reveal the production of  $\text{Fe}_3\text{O}_4/\text{SBA-15}$  nanocomposite.

Figure 2(B) shows the small-angle XRD patterns of neat SBA-15 and  $\text{Fe}_3\text{O}_4/\text{SBA-15}$  nanocomposite. Pure SBA-15 exhibits a strong (1 0 0) diffraction peak with two small peaks (1 1 0) and (2 0 0) associated with a two-dimensional hexagonal  $p6mm$  mesostructure, confirming the highly ordered mesostructure of the silica host. It

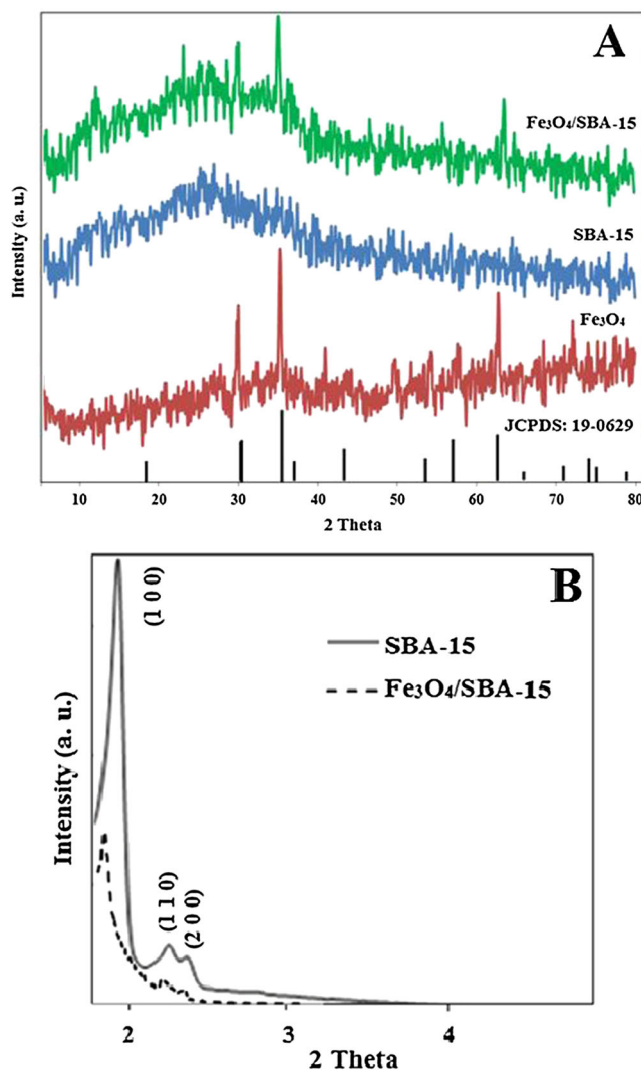


**Figure 2.** (A) Wide-angle XRD patterns of neat SBA-15,  $\text{Fe}_3\text{O}_4$  and  $\text{Fe}_3\text{O}_4/\text{SBA-15}$ . (B) Small-angle XRD patterns of neat SBA-15 and  $\text{Fe}_3\text{O}_4/\text{SBA-15}$ .

can be observed that both of the synthesized samples show the same pattern, which indicates that the hexagonally structured SBA-15 silica with highly ordered mesoporous channels is maintained during the preparation of the heterogeneous catalyst, although the strong peak for  $\text{Fe}_3\text{O}_4/\text{SBA-15}$  compared with SBA-15 is decreased. This could be due to the presence of  $\text{Fe}_3\text{O}_4$  nanoparticles in SBA-15 pores meaning the sizes of pores are smaller than in SBA-15 and the mesostructure of SBA-15 is disordered which leads to weaker reflections. Therefore these changes reveal that the  $\text{Fe}_3\text{O}_4$  nanoparticles are well immobilized in the SBA-15 nanocages.

#### Nitrogen adsorption–desorption isotherms of $\text{Fe}_3\text{O}_4/\text{SBA-15}$

The textural properties of neat SBA-15 and  $\text{Fe}_3\text{O}_4/\text{SBA-15}$  samples were determined using nitrogen adsorption–desorption isotherms at 77 K. As can be seen in Fig. 3, the isotherms of neat SBA-15 and  $\text{Fe}_3\text{O}_4/\text{SBA-15}$  are type IV ( $\text{H}_2$ ) hysteresis loops that are typical for mesoporous materials with ordered channels. Moreover, in comparison with neat SBA-15, Brunauer–Emmett–Teller (BET) surface area and pore volume of  $\text{Fe}_3\text{O}_4/\text{SBA-15}$  are decreased. This indicates the successful incorporation of  $\text{Fe}_3\text{O}_4$  into nanocages of SBA-15.

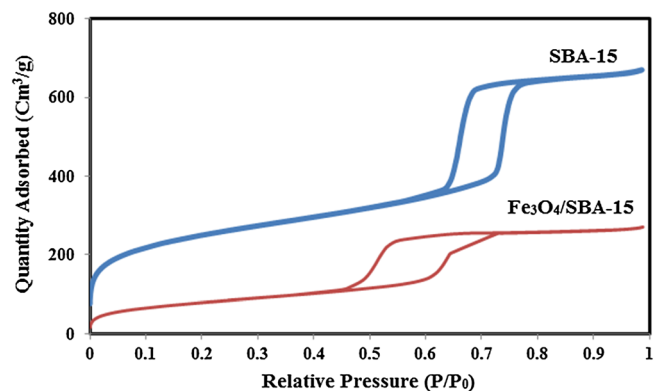


**Figure 3.** Nitrogen adsorption–desorption isotherms of neat SBA-15 and  $\text{Fe}_3\text{O}_4/\text{SBA-15}$ .

#### Magnetic properties of $\text{Fe}_3\text{O}_4/\text{SBA-15}$

The magnetic hysteresis loops for neat SBA-15,  $\text{Fe}_3\text{O}_4$  and  $\text{Fe}_3\text{O}_4/\text{SBA-15}$  are shown in Fig. 4. The magnetic properties of the samples were analysed using vibrating sample magnetometry (VSM) with an applied field  $-7.3 \leq H \leq 7.3$  kOe at room temperature. When the  $\text{Fe}_3\text{O}_4$  is immobilized on SBA-15, the saturation magnetization ( $M_s$ ) is decreased ( $M_s$  of neat SBA-15,  $\text{Fe}_3\text{O}_4$  and  $\text{Fe}_3\text{O}_4/\text{SBA-15}$  is 0.0, 15.2 and  $5.9 \text{ emu g}^{-1}$ , respectively). According to the curves, the remanent magnetization ( $M_r$ ) of  $\text{Fe}_3\text{O}_4$  and  $\text{Fe}_3\text{O}_4/\text{SBA-15}$  is 1.2 and  $0.4 \text{ emu g}^{-1}$ , respectively. The coercivity field of  $\text{Fe}_3\text{O}_4$  and  $\text{Fe}_3\text{O}_4/\text{SBA-15}$  is 8 Oe. Therefore, it can be concluded from the hysteresis loops that  $\text{Fe}_3\text{O}_4$  and  $\text{Fe}_3\text{O}_4/\text{SBA-15}$  are magnetically soft at room temperature.

#### Scanning electron microscopy (SEM) imaging of $\text{Fe}_3\text{O}_4/\text{SBA-15}$

As seen in Fig. 5, the SEM image of SBA-15 exhibits vermicular-shaped particles. The SEM image of magnetite in Fig. 5 shows that the material has a uniform morphology and particle size distribution. The regular morphology indicates that the particles are well crystallized. The SEM image of  $\text{Fe}_3\text{O}_4/\text{SBA-15}$  in Fig. 5 shows the

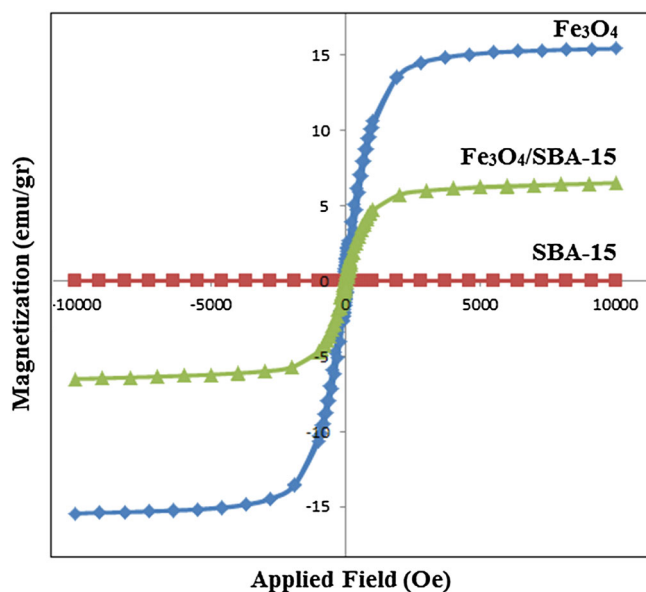


**Figure 4.** Magnetic hysteresis loops for neat SBA-15,  $\text{Fe}_3\text{O}_4$  and  $\text{Fe}_3\text{O}_4/\text{SBA-15}$ .

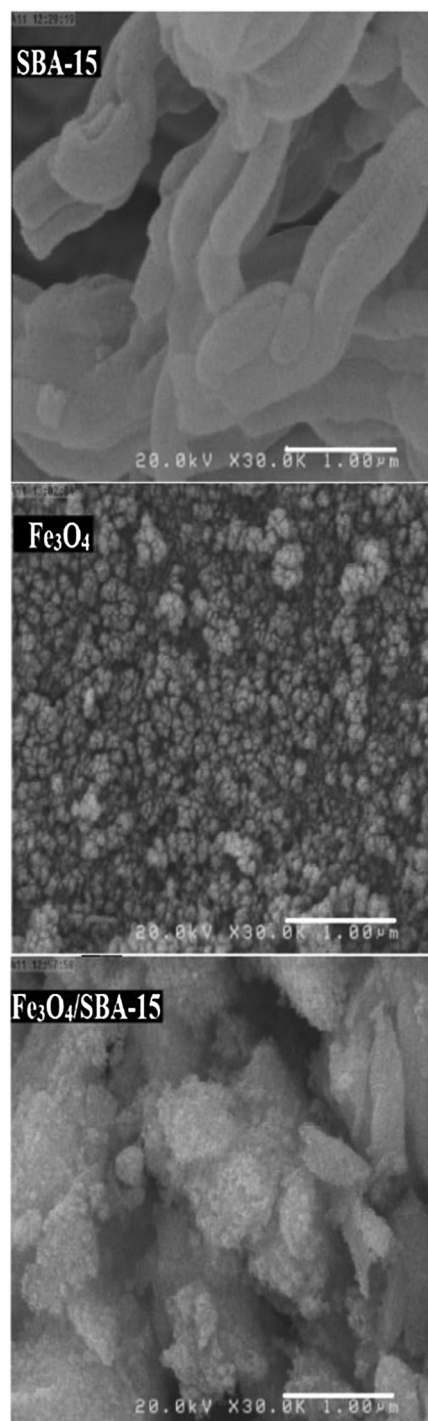


**Figure 5.** SEM images of SBA-15,  $\text{Fe}_3\text{O}_4$  and  $\text{Fe}_3\text{O}_4/\text{SBA-15}$ .

morphology of well-dispersed spherical particles that may be attributed to the presence of magnetite-coated silica nanoparticles. These particles are homogeneous and the average size distribution is about 80 nm. An increased surface roughness is observed in  $\text{Fe}_3\text{O}_4/\text{SBA-15}$ , which may be attributed to the presence of iron oxide particles on the surface of mesoporous silica.

#### Optical properties of $\text{Fe}_3\text{O}_4/\text{SBA-15}$

The ultraviolet (UV)–visible diffuse reflectance spectroscopy (DRS) technique can be utilized to investigate the photocatalytic activity of  $\text{Fe}_3\text{O}_4$

nanoparticles encapsulated in mesoporous SBA-15 silica composites. Figure 6 shows the UV–visible absorption spectra of neat SBA-15 and Fe<sub>3</sub>O<sub>4</sub>/SBA-15. The spectrum of Fe<sub>3</sub>O<sub>4</sub>/SBA-15 exhibits broad absorption bands in both UV and visible regions (200–800 nm). The band gap energy ( $E_g$ ) according to the band maxima of the absorption spectrum was evaluated using the Tauc equation:

$$(\alpha h\nu)^n = B(h\nu - E_g)$$

where  $h\nu$  is the photon energy,  $\alpha$  is the absorption coefficient and  $B$  is a constant value. The value of  $n$  is assigned to transitions, taking different values for allowed and forbidden, direct and indirect transitions. By plotting  $(\alpha h\nu)^n$  versus  $h\nu$  in eV with  $n = 2$  for direct transitions, and then by obtaining the extrapolation point of this curve (inset of Fig. 6), the band gap energy of the product is estimated at about 2.2 eV.

These results reveal that the prepared nanocomposite can also play a suitable role as a photocatalyst under light irradiation. In fact, the presence of Fe<sub>3</sub>O<sub>4</sub> encapsulated in SBA-15 leads to a suitable required energy for electron transfer from valence band to conduction band and, therefore, this synthesized photocatalyst can be activated in the visible region.

### Synthesis of 2,3-Dihydroquinazolin-4(1H)-ones in Presence of Fe<sub>3</sub>O<sub>4</sub>/SBA-15 Nanocatalyst

To investigate the catalytic activity of the prepared Fe<sub>3</sub>O<sub>4</sub>/SBA-15 nanocatalyst in MCRs, a model experiment was carried out. First, to optimize the reaction conditions, the reaction of 1 mmol of each of isatoic anhydride, ammonium acetate and 3-nitrobenzaldehyde was performed as a model reaction in the presence of various solvents (H<sub>2</sub>O, EtOH and CH<sub>3</sub>CN) and under solvent-free conditions. The best results are obtained in refluxing EtOH. The results also confirm that the best amount of Fe<sub>3</sub>O<sub>4</sub>/SBA-15 catalyst is 40 mg mmol<sup>-1</sup> of the raw materials.

To compare Fe<sub>3</sub>O<sub>4</sub>/SBA-15 catalytic activities, the model reaction was also carried out in the presence of various solid, liquid and Lewis acids, such as Amberlyst-21, HOAc and FeCl<sub>3</sub>, respectively, and also Fe<sub>3</sub>O<sub>4</sub> and SiO<sub>2</sub> alone. The best yield is obtained with Fe<sub>3</sub>O<sub>4</sub>/SBA-15. To illustrate the need for the presence of catalyst for these reactions, an experiment was conducted in the absence of Fe<sub>3</sub>O<sub>4</sub>/SBA-15. The yield in this case is a trace amount after 5 h. As a result, Fe<sub>3</sub>O<sub>4</sub>/SBA-15 is an important component of the reaction.

Due to the success of the reaction described above, we investigated the synthesis of 2,3-dihydroquinazolin-4(1H)-one derivatives **4a–j** from MCRs of isatoic anhydride, ammonium acetate and various aldehydes under the optimized reaction conditions. As evident

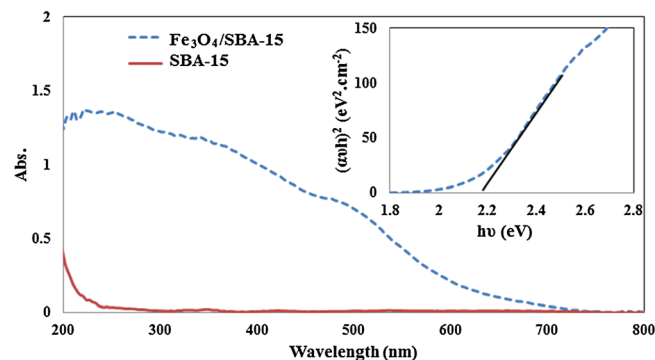


**Figure 6.** UV–visible DRS curves of SBA-15 and Fe<sub>3</sub>O<sub>4</sub>/SBA-15. The inset shows a Tauc plot of Fe<sub>3</sub>O<sub>4</sub>/SBA-15.

from Table 1, the reaction proceeds very efficiently by varying the structure of the aldehyde, and no undesirable side reactions are observed under these reaction conditions.

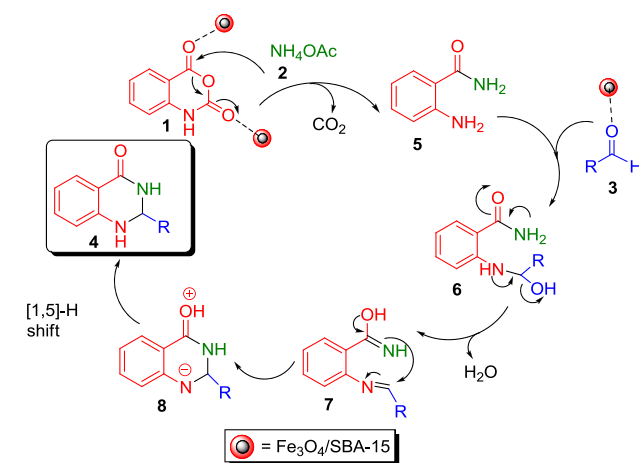
It should be mentioned that both electron-withdrawing and electron-releasing groups, such as NO<sub>2</sub>, COOH, OCH<sub>3</sub> and CH<sub>3</sub>, and also halogens such as Cl suitably react and give the expected products in reasonable times and in good isolated yields.

The aldehyde derivatives containing electron-acceptor groups have a better performance in the reaction to synthesize 2,3-dihydroquinazolin-4(1H)-one. In contrast, the presence of stronger electron-donor groups in benzaldehyde leads to longer reaction time. This is because, for aldehyde containing electron-acceptor groups, the carbon of the carbonyl group is more positive and nucleophilic attack proceeds more easily and the reaction time becomes shorter. The 2-carboxy group is an electron-acceptor group and therefore its activity should be higher and the reactions should occur in shorter times, but due to its steric effect the efficiency of reaction increases.

**Table 1.** Synthesis of 2,3-dihydroquinazolin-4(1H)-ones in the presence of Fe<sub>3</sub>O<sub>4</sub>/SBA-15

| Entry | R  | Product   | Time (h) | Yield (%) <sup>a</sup> | M.p. (°C) |                         |
|-------|--|-----------|----------|------------------------|-----------|-------------------------|
|       |  |           |          |                        | Found     | Reported                |
| 1     | C <sub>6</sub> H <sub>5</sub>                    | <b>4a</b> | 3.5      | 75                     | 217–220   | 218–220 <sup>[30]</sup> |
| 2     | 3-NO <sub>2</sub> C <sub>6</sub> H <sub>4</sub>  | <b>4b</b> | 2.5      | 78                     | 198–200   | 190–192 <sup>[30]</sup> |
| 3     | 4-NO <sub>2</sub> C <sub>6</sub> H <sub>4</sub>  | <b>4c</b> | 3        | 75                     | 198–200   | 198–200 <sup>[31]</sup> |
| 4     | 4-ClC <sub>6</sub> H <sub>4</sub>                | <b>4d</b> | 3        | 75                     | 201–203   | 203–205 <sup>[32]</sup> |
| 5     | 4-OCH <sub>3</sub> C <sub>6</sub> H <sub>4</sub> | <b>4e</b> | 4.5      | 70                     | 192–193   | 192–193 <sup>[32]</sup> |
| 6     | 4-CH <sub>3</sub> C <sub>6</sub> H <sub>4</sub>  | <b>4f</b> | 4        | 73                     | 228–230   | 225–227 <sup>[12]</sup> |
| 7     | 2-COOHC <sub>6</sub> H <sub>4</sub>              | <b>4g</b> | 1.5      | 65                     | 270       | —                       |
| 8     | 2-ClC <sub>6</sub> H <sub>4</sub>                | <b>4h</b> | 3.5      | 75                     | 205–208   | 203–205 <sup>[31]</sup> |
| 9     | 2,4-di-ClC <sub>6</sub> H <sub>3</sub>           | <b>4i</b> | 2.5      | 70                     | 164–165   | 165–167 <sup>[33]</sup> |
| 10    | 4-OHC <sub>6</sub> H <sub>4</sub>                | <b>4j</b> | 4        | 70                     | 205–208   | 210–212 <sup>[34]</sup> |

<sup>a</sup>Isolated yields.



**Scheme 2.** Proposed mechanism for the formation of **4a–j**.

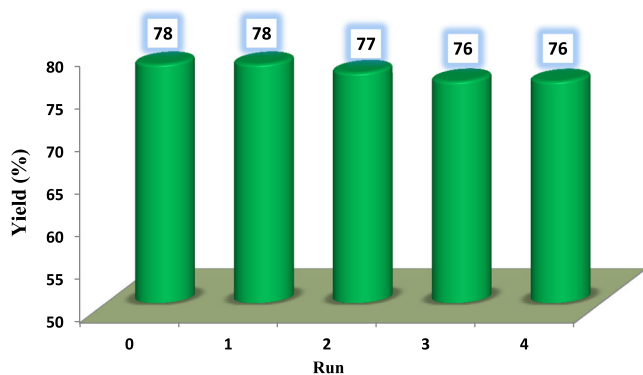


**Figure 7.** Reusability of the  $\text{Fe}_3\text{O}_4/\text{SBA-15}$  catalyst in the synthesis of **4b**.

A possible mechanism for the formation of **4a–j** in the presence of  $\text{Fe}_3\text{O}_4/\text{SBA-15}$  is shown in Scheme 2. The reaction presumably proceeds via the reaction of isatoic anhydride (**1**) and ammonium acetate (**2**) to produce 2-aminobenzamide (**5**) by releasing a  $\text{CO}_2$  molecule. Next, its active  $\text{NH}_2$  group could react with aldehyde **3** to form compound **6**. Then, adduct **6** is cyclized by losing a water molecule, and then an intramolecular nucleophilic attack of **7** affords compound **8**. Finally, a 1,5-hydrogen shift yields the 2,3-dihydroquinazolin-4(1*H*)-ones **4a–j**.

The ability of the heterogeneous nanocatalyst was determined by examining its reusability in the model reaction for the synthesis of 2-(3-nitrophenyl)-2,3-dihydro-4(1*H*)-quinazolinone. After each reaction, the catalyst was completely washed with ethanol and then dried before being used in subsequent runs. The results show that the catalyst can be reused for four consecutive runs without significant loss of its catalytic activity (Fig. 7).

## Conclusions

In summary,  $\text{Fe}_3\text{O}_4/\text{SBA-15}$  as an efficient and eco-friendly heterogeneous composite nanocatalyst was prepared and characterized using FT-IR spectroscopy, DRS, SEM, XRD, VSM and BET analyses. Then, its catalytic activity was investigated in the one-pot multi-component synthesis of 2,3-dihydroquinazolin-4(1*H*)-ones starting from isatoic anhydride, ammonium acetate and various aldehydes under mild reaction condition and easy work-up procedure in ethanol with good yields. The present nanocatalyst was recovered easily and reused without any significant loss of catalytic activity.

## Experimental

### General

All solvents, chemicals and reagents used in this work were of analytical or synthetic grade and used without further purification. XRD measurements were carried out using a JEOL X-ray diffractometer with  $\text{Cu K}\alpha$  radiation. The low-angle XRD patterns of mesoporous materials were obtained with a diffractometer (PANalytical, model X'Pert Pro MPD) with monochromatized  $\text{Cu K}\alpha$  radiation ( $\lambda = 1.54060 \text{ \AA}$ , 40.0 kV, 40.0 mA). Magnetic properties of the samples were obtained using a vibrating sample magnetometer (Lakeshore). The particle morphologies of the as-prepared powders were observed with a Tescan (model Vega II) SEM instrument at 30 kV. Surface area and pore size distribution were determined using the BET multilayer nitrogen

adsorption method in a conventional volumetric technique with a Micromeritics ASAP 2020 instrument. UV–visible DRS spectra were obtained with a Shimadzu MPC-2200 spectrophotometer. Melting points were measured using an Electrothermal 9100 apparatus and are uncorrected. FT-IR spectra were recorded with a Shimadzu FT-IR-8400S spectrometer using KBr pellets for sample preparation.  $^1\text{H}$  NMR spectra were recorded with a Bruker DRX-250 Avance spectrometer at 250 MHz. Elemental analyses were performed with an Elementar Analysen systeme GmbH VarioEL.

All the products were identified by comparison of their spectroscopic and analytical data with those of authentic samples (please see Table 1 and supporting information file).

### Preparation of mesoporous SBA-15

Mesoporous silica SBA-15 material was prepared using tetraethyl orthosilicate (TEOS) as silica precursor and Pluronic P123 (amphiphilic triblock copolymers,  $\text{EO}_{20}\text{PO}_{70}\text{EO}_{20}$ ) as template using the hydrothermal method according to protocols reported previously.<sup>[26–29]</sup>

In a typical procedure, 4.0 g of P123 was dissolved in 100 ml of HCl (2.1 M) and the solution was stirred at  $40^\circ\text{C}$  for 4 h. After dissolution, 6.3 g of TEOS was slowly added to the solution and the water–P123 mixture kept under static conditions at  $40^\circ\text{C}$  for 24 h. Then, the resulting gel was put into a Teflon autoclave for hydrothermal treatment at  $100^\circ\text{C}$  for 48 h. After that, the obtained white solid was filtered and washed with deionized water several times, air-dried at room temperature and then the as-synthesized SBA-15 was calcined at  $550^\circ\text{C}$  for 5 h to remove the surfactant template.

### Preparation of $\text{Fe}_3\text{O}_4/\text{SBA-15}$ nanocomposite

First, 0.0017 mol of  $\text{FeCl}_3 \cdot 6\text{H}_2\text{O}$  (0.482 g) and 0.0008 mol of  $\text{FeCl}_2 \cdot 4\text{H}_2\text{O}$  (0.1774 g) were dissolved in 40 ml of deoxygenated water and stirred for 2 h to make sure that the salts were completely dissolved. Then, 0.5 g of SBA-15 was suspended into the above sol solution. Aqueous ammonia solution was added into the solution under ultrasonication and nitrogen atmosphere, until the pH of the solution reached 9. The mixture was sonicated for 30 min and then left to stand overnight. Finally, the precipitates were collected and washed several times with deionized water and alcohol until the pH decreased to 7. The sample was then heated under nitrogen atmosphere to  $500^\circ\text{C}$  with a heating rate of  $5^\circ\text{C min}^{-1}$  and maintained at  $500^\circ\text{C}$  for 1 h.

### General procedure for synthesis of 2,3-dihydroquinazolin-4(1*H*)-ones **4a–g**

A mixture of **1** (1 mmol), **2** (1 mmol) and an aldehyde **3** (1 mmol) in the presence of  $\text{Fe}_3\text{O}_4/\text{SBA-15}$  nanocatalyst (0.04 g) in 5 ml of EtOH was refluxed in a round-bottomed flask for the appropriate time as indicated in Table 1. After completion of the reaction, as indicated by TLC (ethyl acetate–*n*-hexane, 2:1), the catalyst was removed easily by adsorbing onto the magnetic stirring bar when the stirring was stopped. Then, the reaction solution was filtered off and the residue was purified by washing further with water, and then crystallized from EtOH to give pure crystalline products **4a–g**. The  $\text{Fe}_3\text{O}_4/\text{SBA-15}$  nanocatalyst was then washed with EtOH, air-dried and used directly several times in other fresh reactions without loss of efficiency.

## Acknowledgment

The authors gratefully acknowledge the financial support from the Iran National Science Foundation (INSF) and partial support from the Research Council of the Iran University of Science and Technology.

## References

- [1] S. G. Kwon, T. Hyeon, *Acc. Chem. Res.* **2008**, *41*, 1696–1709.
- [2] B. Julian-Lopez, C. Boissiere, C. Chaneac, D. Grosso, S. Vasseur, S. Miroux, E. Duguet, C. Sanchez, *J. Mater. Chem.* **2007**, *17*, 1563–1569.
- [3] Z. Lu, J. Dai, X. Song, G. Wang, W. Yang, *Colloids Surf. A* **2008**, *317*, 450–456.
- [4] a) S. Rostamizadeh, N. Shadjou, M. Azad, N. Jalali, *Catal. Commun.* **2012**, *26*, 218–224; b) R. Ghahremanzadeh, Z. Rashid, A. H. Zamani, H. Naeimi, *Appl. Catal. A* **2013**, *467*, 270–278; c) H. Aliyan, R. Fazaeli, R. Jalilian, *Appl. Surf. Sci.* **2013**, *276*, 147–153.
- [5] A. M. Alafeefy, A. A. Kadi, O. A. Al-Deeb, K. E. H. El-Tahir, N. A. Al-Jaber, *Eur. J. Med. Chem.* **2010**, *45*, 4947–4952.
- [6] J.-F. Liu, J. Lee, A. M. Dalton, G. Bi, L. Yu, C. M. Baldino, E. McElory, M. Brown, *Tetrahedron Lett.* **2005**, *46*, 1241–1244.
- [7] D. Shi, L. Rong, J. Wang, Q. Zhuang, X. Wang, H. Hu, *Tetrahedron Lett.* **2003**, *44*, 3199–3201.
- [8] a) J. X. Chen, H. Y. Wu, W. K. Su, *Chin. Chem. Lett.* **2007**, *18*, 536–538; b) A. Maleki, S. Shahrokh, in *Proceedings of the 1st International Electronic Conference on Materials*, Sciforum Electronic Conference Series, Vol. 1, **2014**, paper b010.
- [9] A. Shaabani, A. Maleki, H. Mofakham, *Synth. Commun.* **2008**, *38*, 3751–3759.
- [10] L. H. Klemm, T. J. R. Weakley, R. D. Gilbertson, Y.-H. Song, *J. Heterocycl. Chem.* **1998**, *35*, 1269–1273.
- [11] M.-J. Hour, L.-J. Huang, S.-C. Kuo, Y. Xia, K. Bastow, Y. Nakanishi, E. Hamel, K.-H. Lee, *J. Med. Chem.* **2000**, *43*, 4479–4487.
- [12] G. Cai, X. Xu, Z. Li, P. Lu, W. P. Weber, *J. Heterocycl. Chem.* **2002**, *39*, 1271–1272.
- [13] R. J. Abdel-Jalil, W. Voelter, M. Saeed, *Tetrahedron Lett.* **2004**, *45*, 3475–3476.
- [14] C. Balakumar, P. Lamba, D. Pran Kishore, B. Lakshmi Narayana, K. Venkat Rao, K. Rajwinder, A. Raghuram Rao, B. Shireesha, B. Narsaiah, *Eur. J. Med. Chem.* **2010**, *45*, 4904–4913.
- [15] T. Hisano, M. Ichikawa, A. Nakagawa, M. Tsuji, *Chem. Pharm. Bull.* **1975**, *23*, 1910–1916.
- [16] J. Chen, W. Su, H. Wu, M. Liu, C. Jin, *Green Chem.* **2007**, *9*, 972–975.
- [17] V. L. Truong, M. Morrow, *Tetrahedron Lett.* **2010**, *51*, 758–760.
- [18] J. Chen, D. Wu, F. He, M. Liu, H. Wu, J. Ding, W. Su, *Tetrahedron Lett.* **2008**, *49*, 3814–3818.
- [19] I. Mohammadpoor-Baltork, A. R. Khosropour, M. Moghadam, S. Tangestaninejad, V. Mirkhani, S. Baghersad, A. Mirjafari, *C. R. Chim.* **2011**, *14*, 944–952.
- [20] M. Dabiri, P. Salehi, S. Otokesh, M. Baghbazadeh, G. Kozehgary, A. A. Mohammadi, *Tetrahedron Lett.* **2005**, *46*, 6123–6126.
- [21] M. Baghbazadeh, P. Salehi, M. Dabiri, G. Kozehgary, *Synthesis* **2006**, 344–348.
- [22] Z.-H. Zhang, H.-Y. Lu, S.-H. Yang, J.-W. Gao, *J. Comb. Chem.* **2010**, *12*, 643–646.
- [23] M. Wang, T. T. Zhang, Y. Liang, J. J. Gao, *Chin. Chem. Lett.* **2011**, *22*, 1423–1426.
- [24] M. Wang, T. T. Zhang, Y. Liang, J. J. Gao, *Monatsh. Chem.* **2012**, *143*, 835–839.
- [25] a) A. Maleki, *Tetrahedron* **2012**, *68*, 7827–7833; b) A. Maleki, *Tetrahedron Lett.* **2013**, *54*, 2055–2059; c) A. Maleki, *Helv. Chim. Acta* **2014**, *97*, 587–593; d) A. Maleki, N. Ghamari, M. Kamalzare, *RSC Adv.* **2014**, *4*, 9416–9423; e) A. Maleki, M. Kamalzare, *Catal. Commun.* **2014**, *53*, 67–71; f) A. Maleki, *RSC Adv.* **2014**, *4*, 64169–64173; g) A. Maleki, M. Aghaei, N. Ghamari, *Chem. Lett.* **2015**, *44*, 259–261; h) A. Maleki, R. Paydar, *RSC Adv.* **2015**, *5*, 33177–33184.
- [26] Y. J. Li, G. W. Zhou, W. T. Qiao, Y. Y. Wang, *Mater. Sci. Eng. B* **2009**, *162*, 120–126.
- [27] A. Sayari, B. H. Han, Y. Yang, *J. Am. Chem. Soc.* **2004**, *126*, 14348–14349.
- [28] K. Kosuge, T. Sato, N. Kikukawa, M. Takemori, *Chem. Mater.* **2004**, *16*, 899–905.
- [29] Y. Xu, G. Zhou, C. Wu, T. Li, H. Song, *Solid State Sci.* **2011**, *13*, 867–874.
- [30] P. Salehi, M. Dabiri, M. Baghbazadeh, M. Bahramnejad, *Synth. Commun.* **2006**, *36*, 2287–2292.
- [31] a) M. Wang, T. T. Zhang, Z. G. Song, *Chin. Chem. Lett.* **2011**, *22*, 427–430; b) Y. Zong, Y. Zhao, W. Luo, X. H. Yu, J. K. Wang, Y. Pan, *Chin. Chem. Lett.* **2010**, *21*, 778–781.
- [32] J. Chen, D. Wu, F. He, M. Liu, H. Wu, J. Ding, W. Su, *Tetrahedron Lett.* **2008**, *49*, 3814–3818.
- [33] Z. Song, L. Liu, Y. Wang, X. Sun, *Res. Chem. Intermed.* **2012**, *38*, 1091–1099.
- [34] M. Wang, J.-J. Gao, Z.-G. Song, L. Wang, *Org. Prep. Proc. Int.* **2012**, *44*, 159–163.

## Supporting information

Additional supporting information may be found in the online version of this article at the publisher's web-site.